Experimental and theoretical investigations of radiative lifetimes in the *s* and *d* sequences of neutral boron

H. Lundberg,* Z. S. Li, and P. Jönsson†
Department of Physics, Lund Institute of Technology, P.O. Box 118, S-221 00 Lund, Sweden
(Received 1 June 2000; published 7 February 2001)

Radiative lifetimes in the B I $2s^2ns\ ^2S$ ($n \leqslant 7$) and $2s^2nd\ ^2D$ ($n \leqslant 6$) sequences have been measured employing selective laser excitation at vacuum ultraviolet wavelengths. Theoretical calculations were performed using the multiconfiguration Hartree-Fock method. In particular the effect of configuration interaction with the sequence perturbers $2s2p^2\ ^2S$ and ^2D was studied.

DOI: 10.1103/PhysRevA.63.032505 PACS number(s): 32.70.Cs, 42.62.Fi

I. INTRODUCTION

The development of laser spectroscopic techniques has made laser measurements of short radiative lifetimes in the vacuum ultraviolet (VUV) spectral range feasible. High-energy atomic levels can be selectively excited and induced fluorescence captured with high resolution both in time and wavelength. In the present work on lifetimes in the *s* and *d* Rydberg sequences of boron we combined the methods of laser-pulse compression by stimulated Brillouin scattering (SBS) [1] and frequency up conversion using four-wave mixing [2]. As a light atom with only five electrons boron is well suited for comprehensive nonrelativistic calculations. The lifetimes were calculated using the multiconfiguration Hartree-Fock (MCHF) method.

Rydberg sequences in boron show strong irregularities in energy due to configuration interaction. The energy level structure, given in Fig. 1, is similar to that of a one-electron system. The ground configuration is $1s^22s^22p$ and higher states are formed by excitation of the $2p$ electron. In addition, the configuration $1s^22s2p^2$ give rise to a few terms below the ionization energy, ^2S, ^4P, and ^2D. The ^2S and ^2D levels have energies as shown in the figure. The presence of these states causes a perturbation of close-lying levels of the same symmetry. This can be observed as irregularities in the energy positions of the levels. The perturbation can also have a strong effect on lifetime values. In an unperturbed sequence lifetime values can be expected to increase regularly with the principal quantum number.

Radiative lifetimes have previously been studied in Rydberg sequences of the other group III elements Al [3,4], Ga [5], and In [6]. These elements have a similar energy-level structure, but the relative position of the sequence perturbers varies. It is only for boron that the ^2S perturber is below the ionization limit. Furthermore, the ^2D perturber has not been found experimentally in the heavier elements. The state is mixed into the whole *d* sequence.

For boron the strong perturbations make theoretical studies difficult. In particular this is true for the ^2S series, where the position of $2s2p^2\ ^2S$ between $2s^26s\ ^2S$ and $2s^27s\ ^2S$ must be accurately predicted. Calculations of the lifetimes in the *s* and *d* sequences have previously been done using the MCHF method [7]. Due to instabilities in the self-consistent-field procedure only the $2s^2ns\ ^2S$ states below the $2s2p^2\ ^2S$ perturber could be targeted. Improvements in the algorithms now allow the MCHF calculations to be extended further up in the sequence.

The measurements were undertaken using the time-resolved laser-induced fluorescence (LIF) method on boron atoms produced by laser ablation. To obtain the VUV wavelengths, necessary for excitation of the high levels from the ground, sum-difference frequency mixing of two laser beams in a krypton cell was employed. Laser pulses were compressed to 1 ns using SBS in a water cell prior to excitation of investigated levels. Measurements were performed on the $5s$, $6s$, $7s$, $4d$, $5d$, and $6d$ levels in the Rydberg sequences and on the perturber $2s2p^2\ ^2S$. The lower ($n=3$) levels have previously been studied by several investigators mainly using the beam-foil method. One study also includes the ^2S perturber [8]. Levels up to $4s$ and $4d$ have been investigated using laser excitation [9].

II. EXPERIMENTAL METHODS

The radiative lifetimes were measured with the method of selective excitation of an atomic level by wavelength-tuned

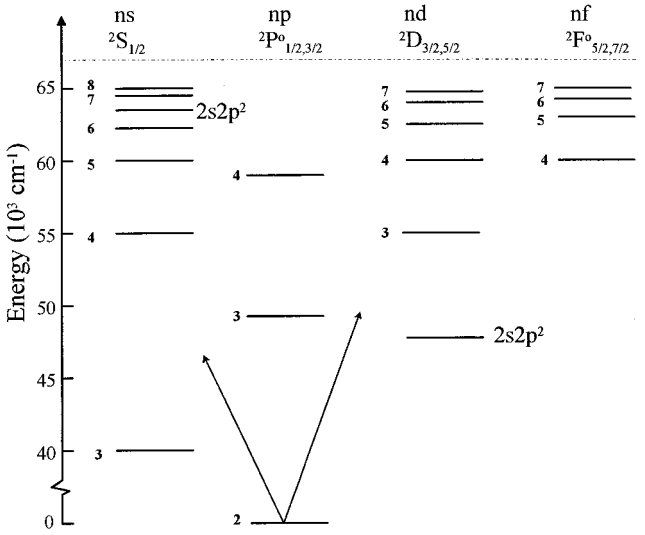

FIG. 1. Energy-level diagram for neutral boron with levels relevant for this investigation included.

*Email address: Hans.Lundberg@fysik.lth.se
†Also at Malmö University, S-205 06 Malmö, Sweden.

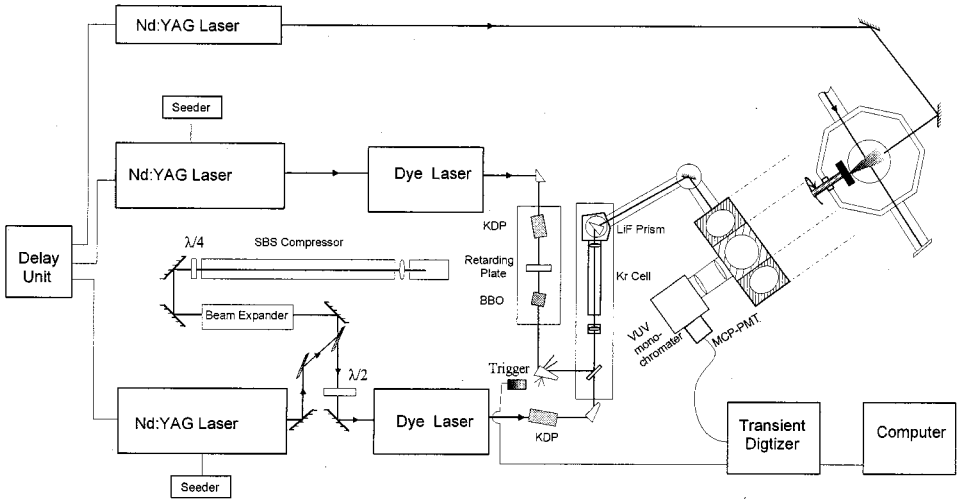

FIG. 2. Experimental setup.

pulsed laser radiation and time-resolved detection of radiation released at the subsequent decay. The experimental setup is shown in Fig. 2. Free boron atoms are produced by focusing a pulsed Nd:YAG (where YAG is yttrium aluminum garnet) laser beam onto a rotating boron target. The laser pulse creates a small plasma, which expands from the target and contains electrons, atoms, and ions of various ionization stages. The laser pulse has duration of 10 ns and a typical energy of 10 mJ. This source has been utilized for a large number of elements and was used, and also examined more thoroughly, in a work on boron [10]. The plasma expands in a shell-like structure with higher velocities for the higher ionization stages. The source has the advantage of high particle densities and the possibility of using populated metastable levels as a starting point for laser excitation. The plasma density and temperature can be adjusted by changing laser energy and beam size on the target. Measurements are performed on atoms or ions in a particular part of the plasma by adjusting the height above the target and the time delay of the excitation pulse.

Tuneable VUV radiation was generated through the process of resonant sum-difference-frequency mixing, $2\omega_1 - \omega_2$, of two UV beams in a krypton gas cell. The two UV beams were overlapped and focused into the cell using an $f=30$-cm achromatic lens. One of the beams, with wavelength 212.55 nm and frequency ω_1, was two-photon resonant with the transition $4p^6\ {}^1S_0 - 4p^5({}^2P_{3/2})5p\ [0\ \frac{1}{2}]\ J=0$ in krypton. The polarization of the gas and the conversion efficiency is enhanced by the resonance. The generated beam, $2\omega_1 - \omega_2$, was tuned by tuning the frequency of the second beam ω_2. The pressure in the cell, optimized on output power of the generated beam, was about 200 mTorr. The three beams were separated by a lithium fluoride prism. After passing the plasma the generated beam was terminated on a window covered with fluorescent sodiumsalicylate.

The two UV beams were produced using two tuneable dye lasers, pumped by two injection-seeded frequency-doubled Nd:YAG lasers, which had pulse powers of about 500 mJ and pulse duration of about 10 ns. One of them pumped a dye laser operated with the dye DCM to give radiation at the wavelength 638 nm. The second harmonic of this radiation was then generated in a KDP crystal and mixed with the fundamental in a BBO crystal to obtain 212.55 nm.

The pulse from the other Nd:YAG laser was shortened by SBS in a water cell. In lifetime measurements the excitation pulse should be shorter than the measured lifetime. The length of the water cell corresponds to half the length of the pulse. The SBS first occurs in the focal point in the generator part of the cell and causes a reflection as from a mirror. This mirror then travels back the amplifier part of the cell with a velocity close to the speed of light. This results in a compression of the pulse to about 1 ns. The loss in pulse energy is about 50%. The compressed pulse pumped a second dye laser operated with different red dyes depending on the requested wavelength of the final VUV radiation. The second dye laser was frequency doubled to ω_2 and made to temporally overlap with the peak of the ω_1 beam. The two Nd:YAG lasers were triggered from a delay generator, which also controlled the plasma-generating laser.

The excitation beam interacted with the boron atoms about 1 cm above the target. Fluorescent light released at the decay was captured using a 0.25-m vacuum monochromator and a multichannel-plate photomultiplier with a rise time of 0.2 ns. The photomultiplier was connected to a digital transient recorder with an analog bandwidth of 1 GHz and real-time sampling rate of 2 G samples/s. The temporal structure of the VUV excitation pulses was recorded with the same detection system by inserting a metal rod into the place of the plasma.

III. MEASUREMENTS

In the measurements level energies were taken from Ref. [11] and detection was performed at the same wavelength as excitation. The resonance lines for the studied states are in the region 156–167 nm. This region was covered using red dyes operated between 586 and 668 nm (first harmonic of the ω_2 beam). The experimental bandwidth, measured by tuning the red dye laser over a transition, was about 0.01 nm, which corresponds to 0.002 nm in VUV. The ${}^2D_{3/2}$ levels can be selectively excited from the ground level ${}^2P_{1/2}$. With exci-

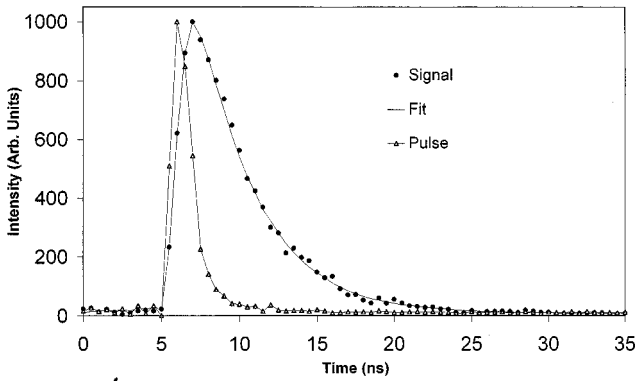

FIG. 3. A fluorescence signal observed at the decay of the $2s2p^2\ ^2S$ level and the excitation laser pulse is shown. The signal is fitted to a convolution of the pulse and an exponential with inverted decay constant of 3.3 ns.

tation from the $^2P_{3/2}$ the fine structure in the ^2D sequence could not be resolved. Both excitation schemes were employed but no difference in decay times was found. This indicates that *LS* coupling is dominant, which is to be expected in a light element as boron.

The energy of the generated beam was estimated to be about 1 μJ. It is given by the intensity of the input beams and the third-order nonlinear susceptibility of the krypton gas. The susceptibility is enhanced when radiation frequencies are close to transition frequencies in the gas. With input beams with powers of a few mJ the conversion efficiency is of the order of 10^{-4}. To obtain a reasonably strong fluorescence it is an advantage to have an atomic source with a high density that sufficiently can compensate for weak excitation beams. It is then, however, important to take care to avoid multiple scattering prolonging observed lifetimes. In the measurements the boron density was changed by changing the delay time between excitation and ablation pulses. For delays longer than 2 μs no systematic effects on the decay times were observed for any level.

In the measurements laser pulses and fluorescence signals were recorded alternately. The curves shown in Fig. 3 represent averages of 1000 pulses. Pulses from the red dye laser, measured with a streak camera, have duration of about 1 ns and pulse-to-pulse fluctuations of typically 20%, somewhat depending on the dye used. The VUV pulses will have similar characteristics. In the figure the laser pulse has a width of about 1.5 ns due to the limit in time response of the detection system. The fluorescence signal is free from both scattered laser light and saturation due to the low energy of the VUV excitation pulse. The lifetimes were evaluated by fitting the fluorescence signal to a convolution of the laser pulse and an exponential. The procedure takes the limited time response into account since the recorded pulse and fluorescence are affected by the same response function. In test measurements the extensively studied lifetime of the Be I $2s2p^1P_1$ level [12] was reproduced.

Several effects, such as collisions and flight out of view, can cause errors in experimental lifetimes. In the measurements attempts were made to actually observe these effects by systematically changing experimental parameters. The final recordings were then made in regions where the setting of these parameters did not affect the lifetime. The final lifetime values are averages from a number of such recordings. The error bars of the values include the equal parts of statistical scattering between different recordings and the possibility of disregarding systematic effects.

IV. THEORY

All the calculations were based on the usual nonrelativistic Hamiltonian with a point nucleus of infinite mass

$$H=\sum_{i=1}^{N}\left(-\frac{1}{2}\nabla_i^2-\frac{Z}{r_i}\right)+\sum_{i<j}\frac{1}{r_{ij}}. \tag{1}$$

In the nonrelativistic multiconfiguration Hartree-Fock (MCHF) method [13] the wave function ψ for a state labeled γLS, where γ represents the configuration and any other quantum number required to specify the state, is approximated by an expansion of configuration state functions (CSF's) with the same *LS* term

$$\Psi(\gamma LS)=\sum_j c_j\Phi(\gamma_j LS). \tag{2}$$

The configuration state functions $\Phi(\gamma LS)$ are antisymmetrized linear combinations of products of spin orbitals,

$$\phi_{nlm_lm_s}=\frac{1}{r}P_{nl}(r)Y_{lm_l}(\theta,\varphi)\xi_{m_s}(\sigma), \tag{3}$$

where the radial functions $P_{nl}(r)$ are represented numerically on a grid. The radial functions are required to be orthonormal. In the multiconfiguration self-consistent field (MCSCF) procedure, both the radial functions and the expansion coefficients are optimized to self-consistency. The former leads to a system of coupled differential equations, one for each radial function, and the latter to a matrix eigenvalue problem. In the present work a modified version of the MCHF package was used with the ability to optimize not only on a single state, but on a weighted linear combination of several states [14], referred to as an extended optimal level (EOL) calculation.

Once the wave functions have been determined, various properties can be computed, including the rates for transitions between different states. When the wave functions for initial and final states are optimized independently, the usual angular momentum theory for evaluating matrix elements cannot be used since the combined orbital set is not orthonormal. To overcome this the orbitals of the initial and final states were transformed to a biorthonormal basis so that the evaluation of the matrix elements can proceed in the usual manner. This transformation is then followed by a transformation of the expansion coefficients to leave the wave functions invariant [15].

V. METHOD OF CALCULATION

EOL calculations were performed for each of the ^2S, ^2P, ^2D, and ^2F symmetries. The ^2P and ^2F Rydberg series are

TABLE I. Theoretical and experimental excitation energies for boron levels. The ^2S levels were adjusted semiempirically.

Term	Calculated energy (cm^{-1})	Adjusted energy (cm^{-1})	Experimental energy (cm^{-1})
$1s^22s^23s\ ^2S$	39 733	39 728	40 040
$1s^22s^24s\ ^2S$	54 692	54 682	55 010
$1s^22s^25s\ ^2S$	59 830	59 810	60 146
$1s^22s^26s\ ^2S$	62 199	62 135	62 482
$1s^22s2p\ ^2S$	64 250	63 217	63 561
$1s^22s^27s\ ^2S$	63 450	63 855	64 156
$1s^22s^23p\ ^2P$	48 302		48 613
$1s^22s^24p\ ^2P$	57 452		57 786
$1s^22s^25p\ ^2P$	61 090		
$1s^22s^26p\ ^2P$	62 914		
$1s^22s2p^2\ ^2D$	47 918		47 857
$1s^22s^23d\ ^2D$	54 480		54 768
$1s^22s^24d\ ^2D$	59 666		59 993
$1s^22s^25d\ ^2D$	62 150		62 485
$1s^22s^26d\ ^2D$	63 506		63 845
$1s^22s^24f\ ^2F$	59 672		60 031
$1s^22s^25f\ ^2F$	62 157		62 517

unaffected by the $1s^22s2p^2$ and the optimization was on the energy average of the reference states $1s^22s^2np\ ^2P$, $n=2$ to 6 and $1s^22s^2ns\ ^2S$, $n=3-5$, respectively. For ^2S the optimization was on the Rydberg series $1s^22s^2ns\ ^2S$ from $n=3-7$ and the perturbing state $1s^22s2p^2\ ^2S$, which lies between $1s^22s^26s\ ^2S$ and $1s^22s^27s\ ^2S$. For ^2D the lowest state is $1s^22s2p^2\ ^2D$ which was optimized together with $1s^22s^2nd\ ^2D$, $n=3-5$. The wave function expansions were obtained with the active space method where configuration state functions of the specified *LS* symmetry are obtained from rules for distributions of electrons to orbitals, and orbital sets are successively increased. In all cases the expansions were over distributions of the type $1s^2n_11_1n_21_2n_31_3$ with *nl* belonging to the active orbital set. For each of the *LS* symmetries the 1*s* core orbital was obtained from an EOL calculation on the reference states and was kept fixed during the remaining calculations. The orbital sets were systematically increased until a satisfactory convergence of the calculated transition rates were obtained. The largest configuration space for the ^2P symmetry consisted of 10 881 CSF's and was built, in addition to the spectroscopic orbitals defining the EOL reference states, from six *s*, *p*, *d*, five *f*, four *g*, and two *h* correlation orbitals.

TABLE II. Admixture of $2s2p^2\ ^2S$ into the ^2S Rydberg states.

Term	Mixing coefficient
$1s^22s^23s\ ^2S$	−0.0809
$1s^22s^24s\ ^2S$	−0.1154
$1s^22s^25s\ ^2S$	−0.1792
$1s^22s^26s\ ^2S$	−0.3443
$1s^22s^27s\ ^2S$	0.5523

TABLE III. Transition rates for the investigated levels. The unit is s^{-1}. The figure in brackets is the power of 10.

Term	$2s^22p\ ^2P$	$2s^23p\ ^2P$	$2s^24p\ ^2P$	$2s^25p\ ^2P$	$2s^26p\ ^2P$	$2s^24f\ ^2F$	$2s^25f\ ^2F$
$2s^23s\ ^2S$	2.516[8]	1.720[7]	2.066[5]	3.291[2]	4.845[3]		
	2.602[8]	1.741[7]	2.142[5]	2.105[2]	7.556[3]		
$2s^24s\ ^2S$	9.982[7]	1.657[7]	2.603[6]	1.633[5]	3.659[4]		
	1.039[8]	1.662[7]	2.590[6]	1.485[5]	2.575[4]		
$2s^25s\ ^2S$	7.975[7]	5.229[6]	3.745[6]	7.006[5]	9.795[4]		
	8.346[7]	5.157[6]	3.646[6]	7.104[5]	8.225[4]		
$2s^26s\ ^2S$	1.271[8]	1.817[6]	8.948[5]	9.933[5]	2.880[5]		
	1.333[8]	1.689[6]	8.261[5]	8.908[5]	2.693[5]		
$2s2p^2\ ^2S$	2.738[8]	6.317[3]	3.207[4]	9.974[3]	5.316[4]		
	2.874[8]	3.266[4]	8.171[4]	4.448[4]	1.889[4]		
$2s^27s\ ^2S$	1.205[8]	1.895[6]	1.186[6]	7.115[5]	4.682[5]		
	1.265[8]	2.132[6]	1.452[6]	9.169[5]	6.224[5]		
$2s2p^2\ ^2D$	3.788[7]	4.155[2]	2.268[2]	1.535[4]	1.820[4]	2.579[6]	1.589[6]
	4.110[7]	4.441[2]	1.697[3]	2.326[4]	2.810[4]	2.594[6]	1.618[6]
$2s^23d\ ^2D$	2.061[8]	1.278[7]	1.673[6]	5.543[5]	2.876[5]	1.209[7]	3.706[6]
	2.078[8]	1.284[7]	1.639[6]	5.281[5]	2.756[5]	1.192[7]	3.644[6]
$2s^24d\ ^2D$	1.008[8]	1.323[3]	2.525[6]	7.379[5]	2.728[5]	8.309[−1]	2.470[6]
	1.019[8]	2.530[3]	2.511[6]	7.815[5]	2.907[5]	3.121[0]	2.544[6]
$2s^25d\ ^2D$	5.421[7]	2.324[5]	9.166[4]	7.526[5]	3.059[5]	6.127[4]	2.420[0]
	5.466[7]	2.499[5]	1.025[5]	7.325[5]	3.323[5]	4.892[4]	9.646[−1]
$2s^26d\ ^2D$	3.225[7]	2.686[5]	2.152[3]	6.265[4]	2.916[5]	2.630[4]	5.014[4]
	3.232[7]	2.851[5]	4.108[3]	6.600[4]	2.731[5]	1.994[4]	4.322[4]

VI. RESULTS AND DISCUSSION

Table I shows the computed excitation energies. Looking at the ^2S symmetry it is seen that the perturbing state $1s^2 2s 2p^2\ ^2S$ is too high relative to the $1s^2 2s^2 6s\ ^2S$ and $1s^2 2s^2 7s\ ^2S$ states of the Rydberg series. This is due to the single $2s$ electron of the perturbing state that is expected to cause a much stronger polarization of the closed $1s$ subshell, an effect not accounted for in the computational model, than any other single electron with higher n and l quantum numbers. Since the position of the perturbing state has a strong influence on the computed transition rates of the higher members of the sequence, the $\langle \Phi(1s^2 2s 2p^2\ ^2S)|H|\Phi(1s^2 2s 2p^2\ ^2S)\rangle$ diagonal element of the Hamiltonian matrix was semiempirically adjusted before diagonalization to give the correct order of the states. The third column of Table I shows the adjusted energies. In Table II the mixing coefficients of the $2s2p^2\ ^2S$ CSF, as obtained from the adjusted calculation, are shown for each of the Rydberg states in the ^2S series. Table III gives the transition rates between the investigated states, computed using the length and velocity forms of the electric dipole operator. The values of the length and velocity forms agree to within a few percent. The exception being transitions with very small rates and transitions involving $1s^2 2s 2p^2\ ^2S$ and $1s^2 2s 2p^2\ ^2D$. The difference for these terms is due to the polarization effects that has not been accounted for in the computational model. In addition there are several cancellations in the transition matrix elements as discussed in Ref. [7].

In Table IV the lifetime values in the length form calculated from the transition rates given in Table III are compared with experimental lifetimes. Earlier experimental values are only given for a laser spectroscopic investigation and for a beam-foil work including the s perturber. For the s sequence the trend of increase in lifetime with principal quantum number is interrupted by the short-lived $2s2p^2\ ^2S$ perturber. The effect is well reproduced in the calculations.

TABLE IV. Experimental and theoretical lifetime values for the s and d Rydberg sequence in neutral boron.

	Lifetime (ns)		
	Experiment		Theory
State	This work	Others	This work
$2s^2 3s\ ^2S$		4.0(2)[a]	3.97
$2s^2 4s\ ^2S$		8.7(4)[a]	8.59
$2s^2 5s\ ^2S$	11.0(6)		11.3
$2s^2 6s\ ^2S$	7.7(4)		7.65
$2s2p^2\ ^2S$	3.3(2)	3.6(3)[b]	3.65
$2s^2 7s\ ^2S$	8.3(4)		8.01
$2s2p^2\ ^2D$		23.1(2)[a]	26.4
$2s^2 3d\ ^2D$		4.7(2)[a] 3.9(5)[b]	4.57
$2s^2 4d\ ^2D$	10.3(5)	10.0(5)[a]	9.68
$2s^2 5d\ ^2D$	17.5(8)		18.1
$2s^2 6d\ ^2D$	31.5(2.0)		30.3

[a]Reference [9], laser-induced fluorescence.
[b]Reference [8], beam-foil.

The present calculation can be improved by including polarization of the closed $1s$ subshell. This would give a better prediction of the position of the perturbing state, partly removing the need for a semiempirical adjustment. Due to limited computational resources no calculations including the $1s$ polarization were attempted.

ACKNOWLEDGMENTS

This work was supported by the Swedish Natural Science Research Council. The authors acknowledge the support from Professor C. Froese Fischer, Professor S. Svanberg, and the Lund Laser Center.

[1] S. Schiemann, W. Ubachs, and W. Hogervorst, IEEE J. Quantum Electron. **33**, 358 (1977).
[2] A. Borsutzky, R. Brünger, and R. Wallenstein, in *Applied Laser Spectroscopy*, edited by W. Demtröder and M. Inguscio (Plenum, New York, 1990), p. 63.
[3] A. W. Weiss, Phys. Rev. A **9**, 1525 (1974).
[4] C. E. Theodosiou, Phys. Rev. A **45**, 7756 (1992).
[5] J. Carlsson, H. Lundberg, W. X. Peng, A. Persson, C.-G. Wahlström, T. Brage, and C. Froese-Fischer, Z. Phys. D: At., Mol. Clusters **3**, 345 (1986).
[6] G. Jönsson, H. Lundberg, and S. Svanberg, Phys. Rev. A **27**, 2930 (1983).
[7] J. Carlsson, P. Jönsson, L. Sturesson, and C. Froese Fischer, Phys. Rev. A **49**, 3426 (1994).
[8] I. Martinson, W. S. Bickel, and A. Ölme, J. Opt. Soc. Am. **60**, 532 (1969).
[9] T. R. O'Brien and J. E. Lawler, Astron. Astrophys. **255**, 420 (1992).
[10] H. Bergström, G. W. Faris, H. Hallstadius, H. Lundberg, A. Persson, and C.-G. Wahlström, Z. Phys. D: At., Mol. Clusters **8**, 17 (1988).
[11] G. A. Odintzova and A. R. Striganov, J. Phys. Chem. Ref. Data **8**, 63 (1979).
[12] A. Weiss, Phys. Rev. A **51**, 1067 (1995).
[13] C. Froese Fischer, T. Brage, and P. Jönsson, *Computational Atomic Structure: An MCHF Approach* (Institute of Physics, Bristol, 1997).
[14] G. Tachiev and C. Froese Fischer, J. Phys. B **32**, 5805 (1999).
[15] J. Olsen, M. Godefroid, P. Jönsson, P. Å. Malmqvist, and C. Froese Fischer, Phys. Rev. E **52**, 4499 (1995).